DEEP SEMANTIC SEGMENTATION OF MANGROVE COMBINING SPATIAL, TEMPORAL AND POLARIZATION FROM SENTINEL-1 TIME SERIES IN THE BRAZILIAN TERRITORY

GABRIEL MATHEUS DE SOUZA MORENO

Dissertation Submitted to Department of Geography

University of Brasilia

In Partial Fulfillment of the Requirements

For the Master's Degree

April 2022

ABSTRACT

The automatic and accurate detection of mangroves from remote sensing data is essential to assist in conservation strategies and decision-making that minimize possible environmental damage, especially for the Brazilian coast with continental dimensions. In this context, segmentation techniques using deep learning are powerful tools with successful applications in several areas of science, achieving results superior to traditional machine learning methods. However, few studies used deep learning for mangrove areas, and none considered time series of radar images. The present research has the following objectives: (a) development of a mangrove dataset for deep learning in the Southeast region of Brazil considering the spatial, temporal, and polarization dimensions; (b) evaluation of U-net architecture models with three backbones different (ResNet -101, VGG16, and Efficient-net-B7); (c) compare the detection capability of Sentinel-1 images using the following VV-only, VH-only, and VV+VH polarizations; and (d) evaluate the number of temporal images for the best detection of targets (29, 15, 8, 4 images), in the case of using both polarizations the number of images doubles. This research uses the annual Sentinel-1 time series for the period 2017-2020. Data labeling used manual interpretation, resulting in 2,886 images with spatial dimensions of 128x128 pixels and their respective annotations (2,136 for training, 450 for validation, and 300 for testing). The best result considered both polarizations (VV+VH), the maximum number of time-series images (29 VV and 29 VH), U-net with the Efficient-net-B7 backbone, and a threshold of 0.75 (97.35 accuracy, 85.77 precision, 84.96 recall, 85.36 F-score, and 74.46 IoU). The entire image classification used a sliding window approach considering five stride values (8, 16, 32, 64, 128 pixels), where the best result was with 8 pixels. The present method is suitable for monitoring mangrove patterns over time, providing subsidies for conserving these ecosystems.

Keywords: mangrove mapping, synthetic aperture radar (SAR), remote sensing, deep learning, convolutional neural networks

TABLE OF CONTENTS

LIST OF FIGURES

LIST OF TABLES

1. INTRODUCTION

Mangrove ecosystems are distributed along the intertidal zones between 30º S to 30º N latitudes, where their structures can survive in seawater, brackish water, and even in the twice ocean water salinity, such as in salt evaporation pools (Giri, 2016; Kuenzer et al., 2011). This environment consists of one of the most productive and biologically complex ecosystems worldwide (Murdiyarso et al., 2015), developing on a gentle slope and including biological and physical multiple processes (Deyoe et al., 2020). The mangroves have a vital role in the coastal zone by providing a wide range of environmental services subdivided into four main categories (Mitra, 2020): provision (food, water, raw material, and medicinal resources), regulation (natural climate disasters, water purification, and detoxification, pollination, erosion, soil fertility, and disease regulation), cultural (recreation, tourism, aesthetics, education, spiritual, heritage, and mental), and support (ecosystem process, life cycle, and biodiversity). Getzner and Islam (2020) performed a meta-analysis of the economic values of mangrove ecosystem services and identified a wide range of values (without conclusive results) but highlighted the economic importance and emphasized the need for conservation management. Anthropogenic factors and global changes have an intense impact on these ecosystems (Asbridge et al., 2015; Carugati et al., 2018), causing significant forest fragmentation (Bryan-Brown et al., 2020) and loss of mangroves (annual loss rates between 0.26 and 0.66) (Hamilton and Casey, 2016). In the period 2000-2016, the global lost mangrove area was 3,363 km^2 (2.1%), representing an average annual rate of 0.13%, with 62% of the mangrove lost due to anthropogenic causes (predominantly by conversion to aquaculture and agriculture) and 38% due to natural causes (shoreline erosion and extreme weather events) (Goldberg et al., 2020). Human impacts decreased by 10% over the period 2000-2016, from 66% in 2005 to 56% in 2016 (Goldberg et al., 2020), likely due to increased emphasis on conservation efforts and a new awareness of the importance of mangroves (Friess et al., 2016; Hakimdavar et al., 2020).

Thus, monitoring and conservation are essential to maintain the functioning of mangrove ecosystems, where up-to-date information on their extent is highly relevant to support decision-making processes (Kuenzer et al., 2011). Most mangrove forests are extensive and isolated areas requiring much effort to access due to temporary flooding, making field observations much more complex and time-consuming (Minh et al., 2019; Walters et al., 2008). The remote sensing monitoring of mangroves has become an

indispensable procedure due to the following factors: it overcomes the limitations of field research, coverage of large areas, low cost, and adds knowledge of processes on a forest and ecosystem scale. Therefore, remote sensing techniques have been used to monitor and evaluate changes in the mangroves, considering spatial distribution, hydrodynamic, morphological, and ecological processes. A large amount of research on mangroves using remote sensing is systematized in several review articles with different focuses: sensors and image processing techniques (Cárdenas et al., 2017; Kuenzer et al., 2011; Maurya et al., 2021); multispectral remote sensing (Thakur et al., 2020); studies based on unmanned aerial vehicles (Zimudzi et al., 2021); research topics (Heumann, 2011; Wang et al., 2019), extent change (Hu et al., 2018); coastal flood risk reduction (Gijsman et al., 2021), land-use change (Sheriza et al., 2021); carbon stock (Dat Pham et al., 2019a), species, structure, and biomass (Dat Pham et al., 2019b); and opportunities and challenges (Giri, 2016). In Brazil, several studies used remote sensing techniques to detect and analyze mangroves (De Souza Pereira et al., 2012; Diniz et al., 2019; Magris and Barreto, 2010; Pelage et al., 2019; Rodrigues and Souza-Filho, 2011; Walfir et al., 2005).

The review developed by Dat Pham et al. (2019b) demonstrates a predominance of optical images in mangrove mapping over SAR or LIDAR images 2010-2018. However, SAR images have the following advantages over optical sensors: the ability to penetrate clouds and smoke that are persistent inconveniences in tropical areas, day and night acquisition, sensitivity to target structure, surface roughness, and dielectric properties (Dat Pham et al., 2019b; Kuenzer et al., 2011; Walters et al., 2008). The main factors for the lower proportion of radar studies are the complexity of the data and the lower availability of free data. The interpretation of radar data in mangrove ecosystems is a complex analysis, where the backscatter signal corresponds to canopy closure and geometry, leaf structure, stem structure, underlying surface component (soil, mudflat, and water), and its dielectric properties (depending on underlying water surfaces, soil, and plant moisture) (Kuenzer et al., 2011). A recent increase in mangrove mapping using SAR is due to the advent of the Sentinel-1 (S-1) constellation with two satellites (1A and 1B) carrying a C-band SAR instrument (5.405 GHz) on board (Torbick et al., 2016). These images have free distribution and high temporal resolution (twelve days for one satellite and six days for the constellation), which is crucial for monitoring.

Besides, the S-1 data promoted the mapping of mangroves from the SAR time series, where the phenological characteristics of the temporal profile allow separating mangrove forests from other types of land use/land cover. However, most mangrove

studies have used the S-1 time series combined with other optical data time series (Ghorbanian et al., 2022; Hu et al., 2020; Zhao and Qin, 2020), eventually only contributing to the generation of the water mask (Chen et al., 2017; Dong et al., 2020).

Recently, deep learning technology presented significant breakthroughs in image processing, mainly because of convolutional neural networks (CNN), which enable an understanding of the different levels of abstraction (Griffiths and Boehm, 2019; Li et al., 2018; Vali et al., 2020). There are many deep learning tasks such as object detection, keypoint detection, semantic segmentation, instance segmentation, and panoptic segmentation (de Carvalho et al., 2022; Hoeser and Kuenzer, 2020; Yu et al., 2018). Usually, remote sensing studies for counting and estimating the objects use instance segmentation, while the amorphous targets use preferentially semantic segmentation, such as burned areas (Arruda et al., 2021; de Bem et al., 2020b) and oil spills (Bianchi et al., 2020; de Moura et al., 2022). Few studies have applied deep learning approaches to mangrove classification, and most have classified small areas (Y. Guo et al., 2021). **Table 1** lists articles published in scientific journals on remote sensing of mangroves using deep learning techniques to date, most of which use optical imaging, with only one study using radar imaging (Ghosh and Behera, 2021). In addition, the deep learning studies for mangroves consider images from a single date, and there are no studies using time series.

Table 1. Studies of mangroves using deep learning techniques.

Article	Mapped Object	Location	Data	Deep Learning Method
(Sun et al., 2019)	Tree species diversity	China	VHR-RGB images and LiDAR points.	AlexNet VGG16 and ResNet50
(Wan et al., 2019)	Species mapping	Hong Kong	WorldView 2	GoogLeNet
(Ghosh and Behera, 2021)	Aboveground biomass estimates of mangroves	Indian	S-1 (coherence and VH backscatter)	DL model
(M. Guo et al., 2021)	Mangrove mapping	China	S-2A (5 original bands and 6 indices)	Mangrove Extraction Network (ME-Net)
(Y. Guo et al., 2021)	Mangrove mapping	The Maritime Silk Road	Landsat	Capsules-Unet
(Li et al., 2021)	Species distribution	Hong Kong	WorldView-3, airborne hyperspectral images, and LiDAR point cloud.	CNN, RF and SVM
(Wan et al., 2021)	Exotic mangrove detection	Hong Kong	WorldView 2	ResNet

The present study aims to provide an effective monitoring procedure using deep learning techniques. In this regard, this study presents the following contributions: (a) one of the first to use deep learning for mapping mangroves, which can guide other researchers to exploit this target, (b) a mangrove dataset in the Brazilian region, (c) a comparison of different Sentinel-1 (S-1) polarization (VV, VH, and VV+VH) considering

annual data in a period 2017-2020. Therefore, this research seeks to fill a knowledge gap in deep learning studies for mangrove mapping using radar time series.

2. MATERIALS AND METHODS

The research can be subdivided into the following steps (**Figure 1**): (a) selection of the study area and acquisition of the S-1 time series for the period 2017-2020; (b) pre-processing; (c) data annotation; (d) evaluation of the deep learning model for the years 2017-2019-2020, comparing the U-net architecture with three backbones (Efficient-net-B7 (Eff-B7), ResNet-101 (R-101) and VGG16) and with three polarization combinations (only VV, only VH, and VV+VH), totaling nine models; (f) analysis of the number of the images (29, 15, 8, and 4 times), considering the best model defined in the previous step; and (g) image reconstruction using the best model and the sliding window with the 2018 image was not used in any previous process to guarantee the independence of the other phases.
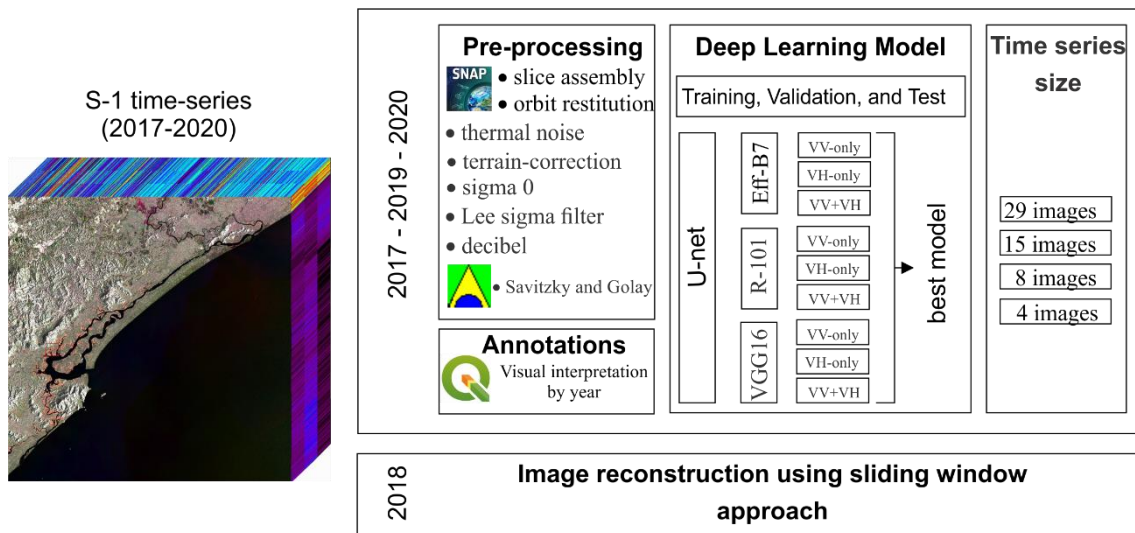
Figure 1. Research methodological flowchart, where Eff-B7 is Efficient-net-B7 and R-101 is ResNet-101.

2.1 Study area

The Cananéia-Iguape Estuarine Complex is within the Atlantic Forest biome and has the most highly conserved mangrove ecosystem in the São Paulo state, Brazil, located in the southern (latitudes between 24º 40' S and 25º 20' S and longitude 48º W) (Cunha-Lignon et al., 2009; Rocha de Souza Pereira et al., 2012) (**Figure 2**). The region of Cananéia-Iguape is marked by the Serra do Mar and coastal plains, formed by systems of lagoons and barriers with inlets and bays that protect from wave action, allowing the development of mangroves (Schaeffer-Novelli et al., 1990).
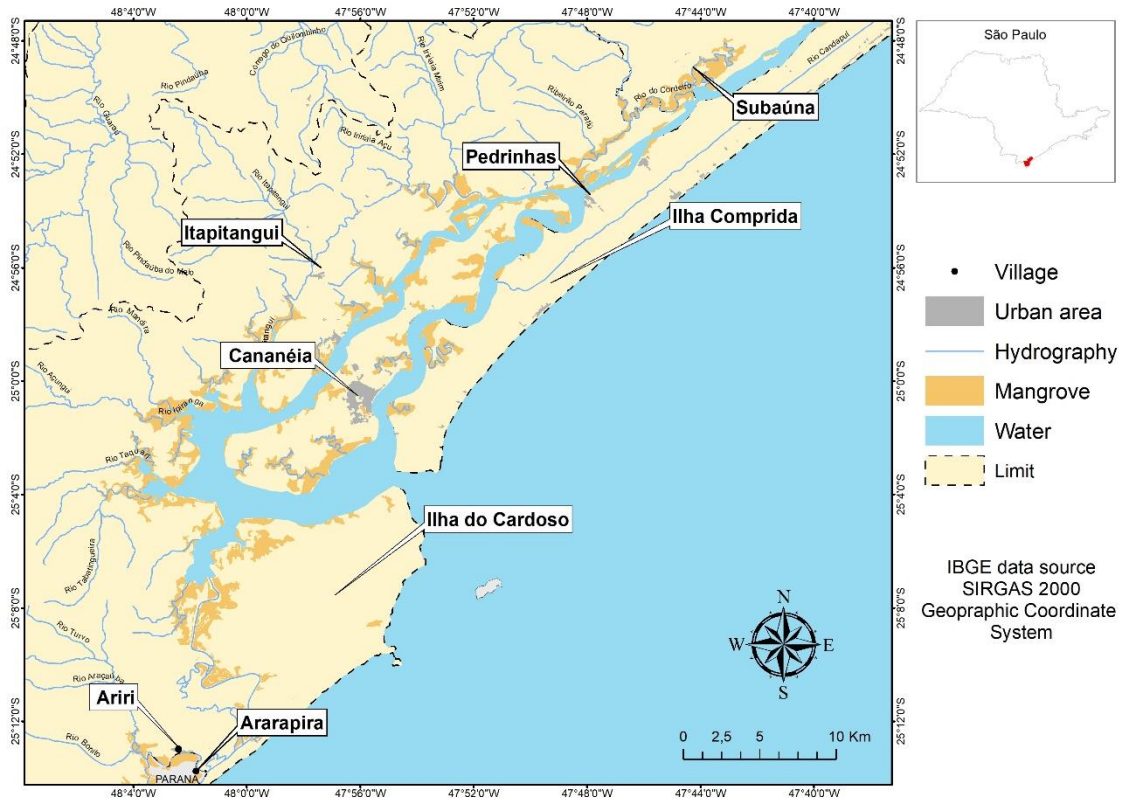
Figure 2. Study area in southeastern Brazil.

Following north to south, the villages inserted close to the complex are called Iguape, Subaúna, Pedrinhas, Itapitangui, Cananéia, Ararapira, and Ariri. Cananéia has the more extensive urban infrastructure in the region, even though it is a remote place. The typic mangrove species found in the region are *Rhizophora mangle*, *Avicennia schaueriana,* and *Laguncularia racemosa* under subtidal, intertidal, and supratidal conditions (Sessegolo and Lana, 1991). *Rhizophora mangle* is the dominant species of mangrove ecosystems (Deyoe et al., 2020), located in intertidal maritime fringe forests and has significant structural development due to the high frequency of flooding in stable depositional sites (Cunha-Lignon et al., 2011).

2.2 Sentinel-1 data

The image acquisition for the period 2017-2020 used the Alaska Satellite Facility Vertex website (ASF, NASA), considering the Interferometric Wide (IW) product with two polarizations VV (vertical transmission and reception) and VH (vertical transmission and horizontal reception) (Torbick et al., 2016). Data pre-processing used Sentinel-1 Toolbox, considering the following steps in SeNtinel Application Platform (SNAP) software (Filipponi, 2019): (1) slice assembly (procedure to merge two slices from

products of an orbit); (2) orbit restitution, (3) thermal noise removal, (4) terrain-correction, based on SRTM digital elevation model (three-second resolution); (5) radiometric calibration (sigma0); (6) Lee Sigma speckle filter (Lee et al., 2009) with a window size of 9×9, a sigma value of 0.9, and a target window size of 5×5; and (7) conversion to decibel (dB).

Complementarily, we apply the Savitzky and Golay (S-G) filter (Savitzky and Golay, 1964) along time series to eliminate interferences over temporal profile. The S-G removes noise and preserves the phenological attributes present in time series (height, maximum and minimum point, shape, and asymmetry) (Abade et al., 2015; Crisóstomo de Castro Filho et al., 2020). With the pre-processed images, we generated temporal cubes for each year in 2017-2020, resulting in 121 bands for each polarization (VH and VV).

2.3 Annotations

The mangrove annotations used the visual interpretation in the QGIS software, having as reference the mapping of the Brazilian Institute of the Environment and Renewable Natural Resources (IBAMA, 2021) and the Global Mangrove Watch extracted from optical and radar by Landsat 8, JERS-1 SAR, ALOS PALSAR, ALOS-2 PALSAR-2 (Bunting et al., 2018; Thomas et al., 2017).

2.4 Training, validation, and test dataset

The training, validation, and test samples had the exact spatial dimensions of 128x128 pixels and temporal dimension of 29 for a single polarization, doubling to 58 times when using both polarizations. The definition of 29 was the smallest number of temporal images within a year in the 2017-2020 interval. The sample selection was random, considering the years 2017, 2019, and 2020. The 2018 data were reserved for an independent evaluation of the image reconstruction from the sliding window (de Albuquerque et al., 2020; de Bem et al., 2020a; Yi et al., 2019). Thus, the dataset reached 2136 samples for training (712 per year), 450 for validation (150 per year), and 300 (100 per year) for testing.

The choice of tiles in the image used the method proposed by Carvalho et al. (2021), which crops the image from point shapefiles from the center of each frame. Using the graphic buffer in the ArcMap software allowed the visualization of possible intersections between the different sets (training, validation, and testing) and avoided data overlap.

2.5 Deep learning approach

The semantic segmentation models aim to classify the image at a pixel level (Yu et al., 2018). Thus, the output image must contain the same dimensions as the original frame. The convolutional neural networks (CNN) (LeCun et al., 2015) play an important role in the deep learning-based architectures, enabling the extraction of features at multiple levels of resolution. This extraction is possible due to multiple convolutions and max-pooling layers (which reduces the dimensions of the images). In this regard, the semantic segmentation architectures must restore the image dimensions, using the upsampling operation.

Despite the wide variety of architectures, the U-net (Ronneberger et al., 2015) is one of the most commonly used, containing an encoder and decoder structure, resulting in a U-shaped model. This model is an adaptation of the fully convolutional network (FCN) (Zhang et al., 2018), in which each encoder block is connected to a decoder block to maintain spatial cohesion and a more precise pixel classification. The encoder section can be replaced by several convolutional neural networks, enabling a better tradeoff between computational resources and predictive power.

The U-net architecture was constant to maintain a more consistent ablation study, but we used three distinct backbones: (1) Efficient-net-B7 (Eff-B7) (Tan and Le, 2019), (2) ResNet-101 (R-101) (He et al., 2016), and (3) VGG16. We evaluated the images using VV-only, VH-only, and VV+VH for each backbone. The models had input dimensions of 128 (height) x 128 (width) x 29 (channels) for the single polarizations and 128 (height) x 128 (width) x 58 (channels) for the combined polarizations. Regarding hyperparameters, we used the Adam optimizer with a learning rate of 0.0001 and batch size of 10.

2.6 Analysis of different sets of temporal images

After defining the best model (architecture and backbone), we analyzed the mangroves' detection with different temporal sets (29, 15, 8, and 4 images). The image selection considered constant intervals over the time series, allowing the characterization of the different periods. Many studies synthesize the time series from a reduced number of images, for example, images of the seasons (e.g., Ghorbanian et al., 2022, 2021). The smaller number of images can decrease the processing time and data acquisition. However, a more extended time series allowed a better definition of phenological behavior and minimization of SAR noise, which helps the DL model detect the intended target. Few studies perform this type of analysis, and a similar study considered different

lengths of S-1 time series for center pivot detection (Albuquerque et al., 2021). The analysis of the number of images in the time series has not yet been carried out to detect mangroves.

2.7 Sliding window approach

The deep learning samples do not correspond to the actual study areas in remote sensing studies. The frames have fixed sizes, whereas the study areas are often larger, requiring post-processing procedures for real-life applications. One of the most used procedures is the sliding window approach, consisting of classifying frames with the exact dimensions as used for training but moving in the X and Y-axis in a predetermined stride value. Usually, the frame edges present a worse classification than the frame centers. A way to attenuate this problem is to use stride values lower than the image's dimensions and average the overlapping pixels. Several studies have evaluated different stride values for better results, showing an increase in the classification metrics (Costa et al., 2021; da Costa et al., 2021; de Albuquerque et al., 2020). The analysis considered step values of 8, 16, 32, 64, and 128 using the best model and polarization configuration.

2.8 Accuracy metrics

The accuracy metrics for supervised semantic segmentation models compare the deep learning prediction with the ground truth image (obtained manually). Nonetheless, the last layer uses a sigmoid activation function, limiting the results from 0 to 1, whereas the ground truth image contains binary values. Thus, it is necessary to establish a threshold value to make a proper comparison. The closer to 1, the stricter the threshold, and the tendency to have false positives decreases, while the threshold closer to 0 tends to reduce false negatives. We considered a conventional threshold of 0.5.

With the defined thresholds, it is possible to define accuracy metrics based on the confusion matrix, which for a binary classification problem has the possible outcomes: (TP) true positives, (TN) true negatives, (FP) false positives, and (FN) false negatives. The most straightforward metric is the overall accuracy, which considers the correct pixels (TP + TN) divided by all (TP+TN+FP+FN). However, this metric may be misleading in imbalanced scenarios since the metric will present high values due to the TNs. The precision metric considers the correctly classified instances (TP) from the classified pixels (TP+FP). Similarly, recall considers the correctly classified pixels from all pixels that should have been classified (TP+FN). These two metrics alone might also be misleading. If the algorithm classifies a single-pixel correctly, the precision would be

100%, or if the algorithm classifies all pixels as 1, the recall would also be 100%. Thus, we use the F-score (harmonic mean between precision and recall) to get a good tradeoff between those two metrics. Finally, one of the primary metrics for semantic segmentation is the intersection over union (IoU). This metric is handy since it considers both false positives and false-negative errors, and it is not prone to class imbalance since it only considers the positive classes, in our case 1. TP divided by TP+FP+FN expresses the IoU.

For the sliding windows approach, since there is an averaging procedure in the probabilistic values for each pixel, it is preferable to use ranking metrics. Thus, we used the average precision (AP), the area under the precision-recall curve, and the area under the receiver operational characteristic (ROC) curve.

3. RESULTS

3.1 Accuracy metrics

Table 2 list the U-net architecture results considering the three backbones (Eff-B7, R-101, and VGG16) with VV, VH, and VV+VH polarizations. The dual-polarization (VV+VH) presented higher results when compared to the single polarizations considering all backbones, showing that the information in each polarization is complementary and may enhance results. Nonetheless, in this scenario, there is an increase in computational resources. First, the dataset requires more data, consuming more memory storage. Second, the deep learning models now need a 58-channel input (twice as much as single polarization), making the training procedure slower.

The Efficient-net-B7 backbone presented the best results when comparing the single polarization, followed by the Resnet-101 and VGG16. The dual-polarization presented better results for all models, and the VV polarization presented better results than the VH for all models. The difference among models was not significant, showing that the patterns to be learned are not too complex, and simpler models such as the VGG16 are highly close in results to the Efficient-net-B7.

Regarding the different thresholds, the models tend to present higher results when reducing the cutoff point. Nonetheless, this difference is minimal, not even reaching 1% for any models. Since this problem has an imbalanced representation of positive and negative instances, the accuracy metrics were very similar for all models and not too informative. In contrast, precision and recall have a tradeoff component; the other tends to go down when one goes up. This can be seen in the VGG16 models with a higher recall rate than the precision rate, even though the F-score is similar to the other models. Finally,

the IoU metric, the primary metric in most studies, presents a similar tendency as the F-score.

Table 2. Accuracy, precision, recall, F-score, and Intersection over Union (IoU) results for the VV-only, VH-only, and VV+VH polarizations considering the U-net architecture with the Efficient-net-B7 (Eff-B7), ResNet-101 (R-101), and VGG16 backbones.

Backbone	Polarization	Accuracy	Precision	Recall	F-score	IoU
		Threshold at 0.75				
Eff-B7	VV	96.81	85.07	78.78	81.80	69.21
	VH	96.72	85.03	77.64	81.17	68.31
	VV+VH	97.35	86.42	84.06	85.22	74.25
R-101	VV	96.69	84.51	77.94	81.09	68.41
	VH	96.58	82.67	78.96	80.78	67.75
	VV+VH	97.27	85.50	84.34	84.92	73.79
VGG 16	VV	96.57	79.37	84.26	81.74	69.12
	VH	96.28	76.41	85.61	80.75	67.72
	VV+VH	97.27	84.35	85.97	85.16	74.15
		Threshold at 0.5				
Eff-B7	VV	96.82	84.72	79.39	81.97	69.44
	VH	96.73	84.67	78.21	81.31	68.51
	VV+VH	97.35	86.10	84.53	85.31	74.38
R-101	VV	96.70	84.24	78.45	81.24	68.41
	VH	96.58	82.23	79.66	80.93	67.95
	VV+VH	97.27	85.12	84.87	85.00	73.91
VGG 16	VV	96.55	78.69	85.12	81.78	69.17
	VH	96.23	75.75	86.25	80.66	67.59
	VV+VH	97.27	83.86	86.66	85.24	74.28
		Threshold at 0.25				
Eff-B7	VV	96.83	84.38	79.98	82.12	69.66
	VH	96.73	84.31	78.76	81.44	68.70
	VV+VH	97.35	85.77	84.96	85.36	74.46
R-101	VV	96.71	83.97	78.93	81.37	68.59
	VH	96.58	81.78	80.35	81.06	68.15
	VV+VH	97.27	84.71	85.40	85.05	73.99
VGG 16	VV	96.51	78.00	85.93	81.77	69.17
	VH	96.18	75.09	86.86	80.54	67.42
	VV+VH	97.26	83.38	87.32	85.30	74.37

Another relevant theme is the inference time and time to train each model. The times to train and inference are the same for the VV-only and VH-only considering that the polarization specifications are equal (same data type, dimensions, and the number of channels) (**Table 3**). The inference time using 58 and 29 input channels is very similar. As remote sensing satellite images are not live-stream, the inference is not as crucial because the difference in the case of milliseconds is not perceptible. Nonetheless, there is a significant difference among the different models, in which the Efficient-net-B7 had the highest inference time, and VGG16 had the lowest, being more than ten times faster. Thus, more complex models have a computational cost in training time. The Efficient-net-B7 takes nearly four minutes to train a single epoch, which for our scenario of 500 epochs takes nearly 33 hours to train the model. There is a significant difference when

comparing training the model with more channels, being nearly three times much faster to train on a single polarization.

Table 3. Inference time and time to train a single epoch for the single and dual polarizations considering the U-net architecture with the Efficient-net-B7 (Eff-B7), ResNet-101 (R-101), and VGG16 backbones.

Backbone	Polarization	Inference time (ms)	Epoch period (min:sec)
Eff-B7	VV+VH	38.99	2:05
	VV or VH	38.76	1:12
R-101	VV+VH	14.45	1:50
	VV or VH	13.73	0:45
VGG16	VV+VH	3.44	1:30
	VV or VH	3.39	0:33

3.2 Evaluation of number of images in the time series composition

Table 4 lists the accuracy metrics of mangrove detection from time series with different numbers of images using the best model (U-net architecture / Efficient-net-B7 and both polarizations). The results showed a reduction in the metrics with the decrease in the number of images. Metric differences are relevant using the entire time series compared to the four-station images, reaching for the distinct threshold values (0.75, 0.5, and 0.25) a Precision difference of 3.5, Recall difference of 5.5, F-score difference of 4.5, IoU difference of 6.6.

Table 4. Accuracy, precision, recall, F-score, and Intersection over Union (IoU) results for the VV+VH polarizations considering different numbers of images in the time series composition (22, 15, 8, and 4) using the best model (U-net architecture with the Efficient-net-B7 backbone).

# Of images	Accuracy	Precision	Recall	F-score	IoU
Threshold at 0.75					
29	97.35	86.42	84.06	85.22	74.25
15	96.88	83.30	82.24	82.77	70.60
8	96.81	85.50	78.25	81.72	69.08
4	96.57	82.91	78.51	80.65	67.58
Threshold at 0.5					
29	97.35	86.1	84.53	85.31	74.38
15	96.88	83.00	82.69	82.84	70.71
8	96.82	85.12	78.91	81.89	69.34
4	96.57	82.60	79.01	80.76	67.74
Threshold at 0.25					
29	97.35	85.77	84.96	85.36	74.46
15	96.88	82.71	83.13	82.92	70.82
8	96.83	84.72	79.52	82.04	69.55
4	96.58	82.30	79.48	80.86	67.88

3.3 Sliding windows results

Table 5 lists the results for the sliding windows considering the different stride values. There is a tradeoff between computational cost and accuracy. The smaller the stride value, the higher the accuracy metrics and computational time. The stride value of

128 has no overlapping pixels, and the higher performance increase is from a 128 to 64 stride value, in more than 10% on PR AUC and 5% in ROC AUC score. Nonetheless, the results increase at a lower rate when reducing the stride.

Table 5. Area under the precision-recall curve and area under the receiver operational characteristic for the four years considering five different stride values.

		Stride value				
Year	Metric	8	16	32	64	128
2017	PR-AUC	79.33	78.63	76.98	74.00	63.86
	ROC	98.41	97.94	97.10	96.06	91.06
	Time (hr:min:sec)	14:50:06	03:45:26	00:55:57	00:14:57	00:05:00

Figure 3 compares for a study area zoom the color compositions of the S-1 temporal bands with and without mangrove vector overlap (terrestrial truth) (**Figure 3a, b**), Sentinel-2 images (Figure 3c), and the results of mangrove mapping using the best model (U-net/Efficient-net-B7, VH+VV polarizations, and 8-step sliding window) (**Figure 3d**).
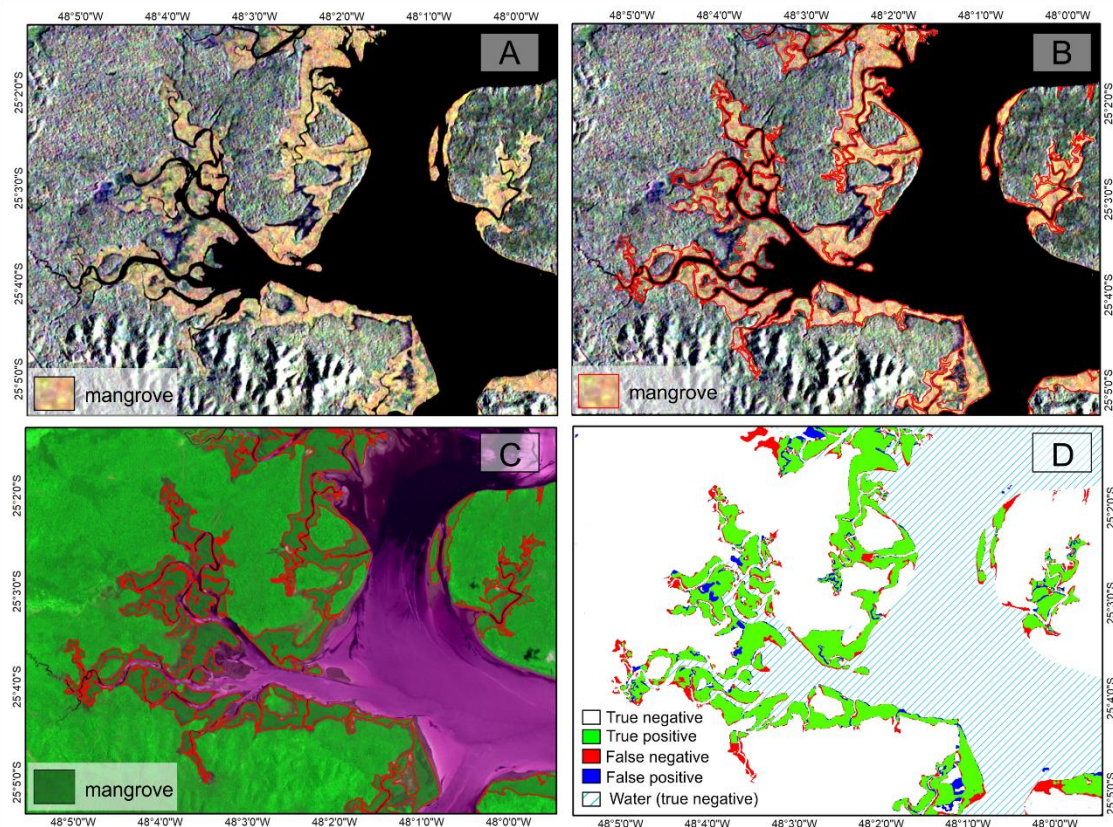
Figure 3. Mangrove images: (A) color composition of VH Sentinel-1 temporal bands (RGB: 04/03/2019, 01/09/2019, and 02/02/2019); (B) mangrove vector (ground truth – red line) on the color composite S-1; (C) mangrove vector over the color composite of Sentinel-2 images (RGB: 4-8-2 bands) dated 12/11/2018; (D) segmentation result

showing true negative (white), false positive (blue), false negative (red) and true positive (green).

Figure 3d shows the error types (FP and FN) and hit areas (TN and TP). False positives always occur at the edges of mangroves in transition to other vegetation, while false negatives usually occur within mangroves in transition zones with bodies of water.

4. DISCUSSION

A consensus in image segmentation and classification is that deep learning achieves better results than traditional and machine learning methods. As it is relatively recent, few remote sensing studies used deep learning for mangrove detection, and among these, most studies were restricted to optical images. To the knowledge of the authors, only one article in a scientific journal used deep learning on radar images for mangrove detection (Ghosh and Behera, 2021). In addition, none of the mangrove articles (with optical or radar images) used time-series and deep learning.

Another significant differential in this mangrove study was the combined use of the spatial, temporal, and polarization (VV and VH) dimensions. Classification based only on the temporal trajectory by pixels has the disadvantage of not depicting the different textures and patterns characteristic of mangroves. At the same time, the use of only images from a single date does not detect the phenological variations that contribute to the differentiation from the other vegetal coverings. Multichannel CNN uses a convolution that considers spatial, textural, and temporal attributes distributed across multiple channels, providing mapping accuracy.

Mangrove mappings with S-1 images were restricted to traditional methods and consistently associated with images from other sensors. Predominantly, mangrove studies with S-1 images used only one date (Pham et al., 2020; Quang et al., 2020; Xia et al., 2020) or synthesized temporal information into a single band by the annual composite (Liu et al., 2021), mean (Xiao et al., 2021), or median and maximum values (Lu and Wang, 2021), always being part of a set of optical and radar images. Some studies with S-1 time series reduced the analysis to 4 images referring to the seasons from the mean (Ghorbanian et al., 2021) or median (Ghorbanian et al., 2022), always associated with the Sentinel-2 (S-2) images. Zhao and Qin (2021) combined S-1 and S-2 time-series, with radar image conversion into quantiles corresponding to 9 percentages. Hu et al. (2020) detected mangroves by combining the S-1 and S-2 time series and the Random Forest method.

An important factor for continuous annual monitoring with deep learning is establishing samples and input data standardization. In this sense, time series of optical images have difficulty obtaining large numbers of images due to the presence of clouds in tropical zones. In opposition, studies with radar time series ensure adequate data acquisition and establish a standard for continued studies.

As in other flooded vegetation (e.g. salt marsh) , the backscatter bands (VV and VH) present complementary information, improving the mapping accuracy (Bem et al., 2021; Lasko et al., 2018). Our results demonstrate that U-net with Efficient-net-B7 produced higher accuracy than ResNet-101 and VGG16. Analysis of segmentation performance using different numbers of temporal images shows a significant difference using 29 times and only four-season images. Besides, the 8-stride sliding windows present better results in reconstructing the entire image than larger intervals, as found in another study (de Albuquerque et al., 2020). Furthermore, the results revealed that only the SAR time series obtained satisfactory results, and multi-source remote sensing data is not crucial for accurate mangrove maps.

5. CONCLUSIONS

Remote sensing is essential to monitor the distribution of mangroves accurately. In this context, deep learning methods reach state of the art for image segmentation. However, few studies use deep learning models for mangrove mapping, where only one study uses radar images, while all the others use optical images. Another knowledge gap with deep learning in mangroves is the use of time series that allow exploring spatial, temporal, and polarization dimensions. Therefore, the present study aimed to evaluate deep learning methods based on CNN to annually monitor and map mangroves from the spatial, temporal, and polarization attributes of Sentinel-1 images. The reuse of DL models for other years requires data standardization, considering the same number of images that depict similar environmental and phenological conditions. Radar images have advantages over optical images due to non-atmospheric interference, guaranteeing data acquisition within a standard. Therefore, the first significant result of the research was the development of a mangrove dataset covering a significant area in southeastern Brazil from the S-1 time series in the period 2017-2020. The spatiotemporal database effectively supports the continuous monitoring of mangrove dynamics in the study area in the coming years. The U-net architecture's precision metrics obtained the best result from the Efficient-net-B7 (Eff-B7) backbone, which surpassed the ResNet-101 (R-101) and the

VGG16. In addition, we obtained better results using the following factors: (a) a combination of the VV and VH polarizations than the single polarization; (b) 29 temporal images than just four-season images; and (c) reconstructing the entire image from 8-step sliding windows instead of larger intervals. As future research, the study can be expanded to the Brazilian coast to optimize policy interventions aimed at the conservation and long-term sustainability of mangroves.

REFERENCE

Abade, N.A., Júnior, O., Guimarães, R.F., de Oliveira, S.N., De Carvalho, O.A., Guimarães, R.F., de Oliveira, S.N., 2015. Comparative Analysis of MODIS Time-Series Classification Using Support Vector Machines and Methods Based upon Distance and Similarity Measures in the Brazilian Cerrado-Caatinga Boundary. Remote Sens. 7, 12160–12191. https://doi.org/10.3390/rs70912160

Albuquerque, A.O., de Carvalho, O.L.F., e Silva, C.R., de Bem, P.P., Trancoso Gomes, R.A., Borges, D.L., Guimarães, R.F., Pimentel, C.M.M., de Carvalho Júnior, O.A., 2021. Instance segmentation of center pivot irrigation systems using multi-temporal Sentinel-1 SAR images. Remote Sens. Appl. Soc. Environ. 23, 100537. https://doi.org/10.1016/j.rsase.2021.100537

Arruda, V.L.S., Piontekowski, V.J., Alencar, A., Pereira, R.S., Matricardi, E.A.T., 2021. An alternative approach for mapping burn scars using Landsat imagery, Google Earth Engine, and Deep Learning in the Brazilian Savanna. Remote Sens. Appl. Soc. Environ. 22, 100472. https://doi.org/10.1016/j.rsase.2021.100472

Asbridge, E., Lucas, R., Accad, A., Dowling, R., 2015. Mangrove Response to Environmental Changes Predicted Under Varying Climates: Case Studies from Australia. Curr. For. Reports 1, 178–194. https://doi.org/10.1007/s40725-015-0018-4

Bem, P.P. de, de Carvalho Júnior, O.A., Carvalho, O.L.F. de, Gomes, R.A.T., Guimarães, R.F., Pimentel, C.M.M.M., 2021. Irrigated rice crop identification in Southern Brazil using convolutional neural networks and Sentinel-1 time series. Remote Sens. Appl. Soc. Environ. 24. https://doi.org/10.1016/j.rsase.2021.100627

Bianchi, F.M., Espeseth, M.M., Borch, N., 2020. Large-Scale Detection and Categorization of Oil Spills from SAR Images with Deep Learning. Remote Sens. 12, 2260. https://doi.org/10.3390/rs12142260

Bryan-Brown, D.N., Connolly, R.M., Richards, D.R., Adame, F., Friess, D.A., Brown, C.J., 2020. Global trends in mangrove forest fragmentation. Sci. Rep. 10, 1–8. https://doi.org/10.1038/s41598-020-63880-1

Bunting, P., Rosenqvist, A., Lucas, R.M., Rebelo, L.M., Hilarides, L., Thomas, N., Hardy, A.,

Itoh, T., Shimada, M., Finlayson, C.M., 2018. The global mangrove watch - A new 2010 global baseline of mangrove extent. Remote Sens. 10. https://doi.org/10.3390/rs10101669

Cárdenas, N.Y., Joyce, K.E., Maier, S.W., 2017. Monitoring mangrove forests: Are we taking full advantage of technology? Int. J. Appl. Earth Obs. Geoinf. 63, 1–14. https://doi.org/10.1016/j.jag.2017.07.004

Carugati, L., Gatto, B., Rastelli, E., Lo Martire, M., Coral, C., Greco, S., Danovaro, R., 2018. Impact of mangrove forests degradation on biodiversity and ecosystem functioning. Sci. Rep. 8, 1–11. https://doi.org/10.1038/s41598-018-31683-0

Carvalho, O.L.F. de, de Carvalho Júnior, O.A., Albuquerque, A.O. de, Bem, P.P. de, Silva, C.R., Ferreira, P.H.G., Moura, R. dos S. de, Gomes, R.A.T., Guimarães, R.F., Borges, D.L., 2021. Instance Segmentation for Large, Multi-Channel Remote Sensing Imagery Using Mask-RCNN and a Mosaicking Approach. Remote Sens. 13, 39. https://doi.org/10.3390/rs13010039

Chen, B., Xiao, X., Li, X., Pan, L., Doughty, R., Ma, J., Dong, J., Qin, Y., Zhao, B., Wu, Z., Sun, R., Lan, G., Xie, G., Clinton, N., Giri, C., 2017. A mangrove forest map of China in 2015: Analysis of time series Landsat 7/8 and Sentinel-1A imagery in Google Earth Engine cloud computing platform. ISPRS J. Photogramm. Remote Sens. 131, 104–120. https://doi.org/10.1016/j.isprsjprs.2017.07.011

Costa, M.V.C.V. da, Carvalho, O.L.F. de, Orlandi, A.G., Hirata, I., Albuquerque, A.O. De, Silva, F.V. e, Guimarães, R.F., Gomes, R.A.T., Júnior, O.A. de C., 2021. Remote Sensing for Monitoring Photovoltaic Solar Plants in Brazil Using Deep Semantic Segmentation. Energies 14, 2960. https://doi.org/10.3390/en14102960

Crisóstomo de Castro Filho, H., Abílio de Carvalho Júnior, O., Ferreira de Carvalho, O.L., Pozzobon de Bem, P., dos Santos de Moura, R., Olino de Albuquerque, A., Rosa Silva, C., Guimarães Ferreira, P.H., Fontes Guimarães, R., Trancoso Gomes, R.A., de Castro Filho, H.C., de Carvalho Júnior, O.A., de Carvalho, O.L.F., de Bem, P.P., dos Santos de Moura, R., Olino de Albuquerque, A., Rosa Silva, C., Guimarães Ferreira, P.H., Guimarães, R.F., Gomes, R.A.T., 2020. Rice Crop Detection Using LSTM, Bi-LSTM, and Machine Learning Models from Sentinel-1 Time Series. Remote Sens. 12, 2655. https://doi.org/10.3390/rs12162655

Cunha-Lignon, M., Coelho, C., Almeida, R., Menghini, R., Correa, F., Schaeffer-Novelli, Y., Cintrón-Molero, G., Dahdouh-Guebas, F., 2009. Mangrove forests and sedimentary processes on the South Coast of São Paulo State (Brazil). J. Coast. Res. 405–409.

Cunha-Lignon, M., Coelho, C., Almeida, R., Menghini, R.P., Schaeffer-Novelli, Y., Cintrón, G., Dahdouh-Guebas, F., 2011. Characterisation of mangrove forest types in view of conservation and management: A review of mangals at the Cananéia region, São Paulo State, Brazil. J. Coast. Res. 349–353.

da Costa, L.B., de Carvalho, O.L.F., de Albuquerque, A.O., Gomes, R.A.T., Guimarães, R.F., de Carvalho Júnior, O.A., 2021. Deep semantic segmentation for detecting eucalyptus planted forests in the Brazilian territory using Sentinel-2 imagery. Geocarto Int. 0, 1–13. https://doi.org/10.1080/10106049.2021.1943009

Dat Pham, T., Xia, J., Thang Ha, N., Tien Bui, D., Nhu Le, N., Tekeuchi, W., 2019a. A review of remote sensing approaches for monitoring blue carbon ecosystems: Mangroves, sea grasses and salt marshes during 2010–2018. Sensors (Switzerland) 19. https://doi.org/10.3390/s19081933

Dat Pham, T., Yokoya, N., Bui, D.T., Yoshino, K., Friess, D.A., 2019b. Remote sensing approaches for monitoring mangrove species, structure, and biomass: Opportunities and challenges. Remote Sens. 11, 1–24. https://doi.org/10.3390/rs11030230

de Albuquerque, A.O., de Carvalho Júnior, O.A., Carvalho, O.L.F. de, de Bem, P.P., Ferreira, P.H.G., de Moura, R. dos S., Silva, C.R., Trancoso Gomes, R.A., Fontes Guimarães, R., 2020. Deep Semantic Segmentation of Center Pivot Irrigation Systems from Remotely Sensed Data. Remote Sens. 12, 2159. https://doi.org/10.3390/rs12132159

de Bem, P.P., de Carvalho Júnior, O., Fontes Guimarães, R., Trancoso Gomes, R., 2020a. Change Detection of Deforestation in the Brazilian Amazon Using Landsat Data and Convolutional Neural Networks. Remote Sens. 12, 901. https://doi.org/10.3390/rs12060901

de Bem, P.P., de Carvalho Júnior, O.A.A., de Carvalho, O.L.F., Gomes, R.A.T., Fontes Guimarães, R., Guimarães, R.F., 2020b. Performance Analysis of Deep Convolutional Autoencoders with Different Patch Sizes for Change Detection from Burnt Areas. Remote Sens. 12, 2576. https://doi.org/10.3390/RS12162576

de Carvalho, O.L.F., de Carvalho Júnior, O.A., Silva, C.R. e, de Albuquerque, A.O., Santana, N.C., Borges, D.L., Gomes, R.A.T., Guimarães, R.F., 2022. Panoptic Segmentation Meets Remote Sensing. Remote Sens. 14, 965. https://doi.org/10.3390/rs14040965

de Moura, N.V.A., de Carvalho, O.L.F., Gomes, R.A.T., Guimarães, R.F., de Carvalho Júnior, O.A., 2022. Deep-water oil-spill monitoring and recurrence analysis in the Brazilian territory using Sentinel-1 time series and deep learning. Int. J. Appl. Earth Obs. Geoinf. 107, 102695. https://doi.org/10.1016/j.jag.2022.102695

De Souza Pereira, F.R., Kampel, M., Cunha-Lignon, M., 2012. Mapping of mangrove forests on the southern coast of São Paulo, Brazil, using synthetic aperture radar data from ALOS/PALSAR. Remote Sens. Lett. 3, 567–576. https://doi.org/10.1080/01431161.2011.641511

Deyoe, H., Lonard, R.I., Judd, F.W., Stalter, R., Feller, I., 2020. Biological Flora of the Tropical and Subtropical Intertidal Zone: Literature Review for Rhizophora mangle L. J. Coast. Res. 36, 857–884. https://doi.org/10.2112/JCOASTRES-D-19-00088.1

Diniz, C., Cortinhas, L., Nerino, G., Rodrigues, J., Sadeck, L., Adami, M., Souza-Filho, P.W.M.,

2019. Brazilian mangrove status: Three decades of satellite data analysis. Remote Sens. 11. https://doi.org/10.3390/rs11070808

Dong, D., Wang, C., Yan, J., He, Q., Zeng, J., Wei, Z., 2020. Combing Sentinel-1 and Sentinel-2 image time series for invasive Spartina alterniflora mapping on Google Earth Engine: A case study in Zhangjiang Estuary. J. Appl. Remote Sens. 14, 044504. https://doi.org/10.1117/1.JRS.14.044504

Filipponi, F., 2019. Sentinel-1 GRD Preprocessing Workflow. Proceedings 18, 11. https://doi.org/10.3390/ecrs-3-06201

Friess, D.A., Thompson, B.S., Brown, B., Amir, A.A., Cameron, C., Koldewey, H.J., Sasmito, S.D., Sidik, F., 2016. Policy challenges and approaches for the conservation of mangrove forests in Southeast Asia. Conserv. Biol. 30, 933–949. https://doi.org/10.1111/cobi.12784

Getzner, M., Islam, M.S., 2020. Ecosystem services of mangrove forests: Results of a meta-analysis of economic values. Int. J. Environ. Res. Public Health 17, 1–13. https://doi.org/10.3390/ijerph17165830

Ghorbanian, A., Ahmadi, S.A., Amani, M., Mohammadzadeh, A., Jamali, S., 2022. Application of Artificial Neural Networks for Mangrove Mapping Using Multi-Temporal and Multi-Source Remote Sensing Imagery. Water 14, 244. https://doi.org/10.3390/w14020244

Ghorbanian, A., Zaghian, S., Asiyabi, R.M., Amani, M., Mohammadzadeh, A., Jamali, S., 2021. Mangrove ecosystem mapping using Sentinel-1 and Sentinel-2 satellite images and random forest algorithm in google earth engine. Remote Sens. 13, 1–18. https://doi.org/10.3390/rs13132565

Ghosh, S.M., Behera, M.D., 2021. Aboveground biomass estimates of tropical mangrove forest using Sentinel-1 SAR coherence data - The superiority of deep learning over a semi-empirical model. Comput. Geosci. 150, 104737. https://doi.org/10.1016/j.cageo.2021.104737

Gijsman, R., Horstman, E.M., van der Wal, D., Friess, D.A., Swales, A., Wijnberg, K.M., 2021. Nature-Based Engineering: A Review on Reducing Coastal Flood Risk With Mangroves. Front. Mar. Sci. 8. https://doi.org/10.3389/fmars.2021.702412

Giri, C., 2016. Observation and Monitoring of Mangrove Forests Using Remote Sensing: Opportunities and Challenges. Remote Sens. 8, 783. https://doi.org/10.3390/rs8090783

Goldberg, L., Lagomasino, D., Thomas, N., Fatoyinbo, T., 2020. Global declines in human-driven mangrove loss. Glob. Chang. Biol. 26, 5844–5855. https://doi.org/10.1111/gcb.15275

Griffiths, D., Boehm, J., 2019. A Review on deep learning techniques for 3D sensed data classification. Remote Sens. 11. https://doi.org/10.3390/rs11121499

Guo, M., Yu, Z., Xu, Y., Huang, Y., Li, C., 2021. ME-Net: A Deep Convolutional Neural Network for Extracting Mangrove Using Sentinel-2A Data. Remote Sens. 13, 1292. https://doi.org/10.3390/rs13071292

Guo, Y., Liao, J., Shen, G., 2021. Mapping large-scale mangroves along the maritime silk road from 1990 to 2015 using a novel deep learning model and landsat data. Remote Sens. 13, 1–20. https://doi.org/10.3390/rs13020245

Hakimdavar, R., Hubbard, A., Policelli, F., Pickens, A., Hansen, M., Fatoyinbo, T., Lagomasino, D., Pahlevan, N., Unninayar, S., Kavvada, A., Carroll, M., Smith, B., Hurwitz, M., Wood, D., Uz, S.S., 2020. Monitoring water-related ecosystems with earth observation data in support of Sustainable Development Goal (SDG) 6 reporting. Remote Sens. 12. https://doi.org/10.3390/rs12101634

Hamilton, S.E., Casey, D., 2016. Creation of a high spatio-temporal resolution global database of continuous mangrove forest cover for the 21st century (CGMFC-21). Glob. Ecol. Biogeogr. 25, 729–738. https://doi.org/10.1111/geb.12449

He, K., Zhang, X., Ren, S., Sun, J., 2016. Deep Residual Learning for Image Recognition, in: 2016 IEEE Conference on Computer Vision and Pattern Recognition (CVPR). IEEE, Las Vegas, NV, USA, pp. 770–778. https://doi.org/10.1109/CVPR.2016.90

Heumann, B.W., 2011. Satellite remote sensing of mangrove forests: Recent advances and future opportunities. Prog. Phys. Geogr. 35, 87–108. https://doi.org/10.1177/0309133310385371

Hoeser, T., Kuenzer, C., 2020. Object Detection and Image Segmentation with Deep Learning on Earth Observation Data: A Review-Part I: Evolution and Recent Trends. Remote Sens. 12, 1667. https://doi.org/10.3390/rs12101667

Hu, L., Li, W., Xu, B., 2018. The role of remote sensing on studying mangrove forest extent change. Int. J. Remote Sens. 39, 6440–6462. https://doi.org/10.1080/01431161.2018.1455239

Hu, L., Xu, N., Liang, J., Li, Z., Chen, L., Zhao, F., 2020. Advancing the mapping of mangrove forests at national-scale using Sentinel-1 and Sentinel-2 time-series data with Google Earth Engine: A case study in China. Remote Sens. 12. https://doi.org/10.3390/RS12193120

IBAMA, 2021. Vegetação de Mangue brasileira [WWW Document]. 2021. URL https://dadosabertos.ibama.gov.br/dataset/vegetacao-de-mangue-brasileira (accessed 3.26.22).

Kuenzer, C., Bluemel, A., Gebhardt, S., Quoc, T.V., Dech, S., 2011. Remote sensing of mangrove ecosystems: A review, Remote Sensing. https://doi.org/10.3390/rs3050878

Lasko, K., Vadrevu, K.P., Tran, V.T., Justice, C., 2018. Mapping Double and Single Crop Paddy Rice with Sentinel-1A at Varying Spatial Scales and Polarizations in Hanoi, Vietnam. IEEE J. Sel. Top. Appl. Earth Obs. Remote Sens. 11, 498–512. https://doi.org/10.1109/JSTARS.2017.2784784

LeCun, Y., Bengio, Y., Hinton, G., 2015. Deep learning. Nature 521, 436–444.

Lee, J. Sen, Wen, J.H., Ainsworth, T.L., Chen, K.S., Chen, A.J., 2009. Improved sigma filter for speckle filtering of SAR imagery. IEEE Trans. Geosci. Remote Sens. 47, 202–213.

https://doi.org/10.1109/TGRS.2008.2002881

Li, Q., Wong, F.K.K., Fung, T., 2021. Mapping multi-layered mangroves from multispectral, hyperspectral, and LiDAR data. Remote Sens. Environ. 258, 112403. https://doi.org/10.1016/j.rse.2021.112403

Li, Y., Zhang, H., Xue, X., Jiang, Y., Shen, Q., 2018. Deep learning for remote sensing image classification: A survey. WIREs Data Min. Knowl. Discov. 8. https://doi.org/10.1002/widm.1264

Liu, X., Fatoyinbo, T.E., Thomas, N.M., Guan, W.W., Zhan, Y., Mondal, P., Lagomasino, D., Simard, M., Trettin, C.C., Deo, R., Barenblitt, A., 2021. Large-Scale High-Resolution Coastal Mangrove Forests Mapping Across West Africa With Machine Learning Ensemble and Satellite Big Data. Front. Earth Sci. 8, 1–15. https://doi.org/10.3389/feart.2020.560933

Lu, Y., Wang, L., 2021. How to automate timely large-scale mangrove mapping with remote sensing. Remote Sens. Environ. 264, 112584. https://doi.org/10.1016/j.rse.2021.112584

Magris, R.A., Barreto, R., 2010. Mapping and assessment of protection of mangrove habitats in Brazil. Panam. J. Aquat. Sci. 5, 546–556.

Maurya, K., Mahajan, S., Chaube, N., 2021. Remote sensing techniques: mapping and monitoring of mangrove ecosystem—a review. Complex Intell. Syst. 7, 2797–2818. https://doi.org/10.1007/s40747-021-00457-z

Minh, H.V.T., Avtar, R., Mohan, G., Misra, P., Kurasaki, M., 2019. Monitoring and mapping of rice cropping pattern in flooding area in the Vietnamese Mekong delta using Sentinel-1A data: A case of an Giang province. ISPRS Int. J. Geo-Information 8. https://doi.org/10.3390/ijgi8050211

Mitra, A., 2020. Ecosystem Services of Mangroves: An Overview, in: Mangrove Forests in India. Springer International Publishing, Cham, pp. 1–32. https://doi.org/10.1007/978-3-030-20595-9_1

Murdiyarso, D., Purbopuspito, J., Kauffman, J.B., Warren, M.W., Sasmito, S.D., Donato, D.C., Manuri, S., Krisnawati, H., Taberima, S., Kurnianto, S., 2015. The potential of Indonesian mangrove forests for global climate change mitigation. Nat. Clim. Chang. 5, 1089–1092. https://doi.org/10.1038/nclimate2734

Pelage, L., Domalain, G., Lira, A.S., Travassos, P., Frédou, T., 2019. Coastal Land Use in Northeast Brazil: Mangrove Coverage Evolution Over Three Decades. Trop. Conserv. Sci. 12. https://doi.org/10.1177/1940082918822411

Pham, Tien Dat, Yokoya, N., Xia, J., Ha, N.T., Le, N.N., Nguyen, T.T.T., Dao, T.H., Vu, T.T.P., Pham, Tien Duc, Takeuchi, W., 2020. Comparison of machine learning methods for estimating mangrove above-ground biomass using multiple source remote sensing data in the red river delta biosphere reserve, Vietnam. Remote Sens. 12, 1–24. https://doi.org/10.3390/RS12081334

Quang, N.H., Quinn, C.H., Stringer, L.C., Carrie, R., Hackney, C.R., Van Hue, L.T., Tan, D. Van, Thanh Nga, P.T., 2020. Multi-decadal changes in mangrove extent, age and species in the Red River Estuaries of Viet Nam. Remote Sens. 12. https://doi.org/10.3390/rs12142289

Rocha de Souza Pereira, F., Kampel, M., Cunha-Lignon, M., 2012. Mapping of mangrove forests on the southern coast of São Paulo, Brazil, using synthetic aperture radar data from ALOS/PALSAR. Remote Sens. Lett. 3, 567–576. https://doi.org/10.1080/01431161.2011.641511

Rodrigues, S.W.P., Souza-Filho, P.W.M., 2011. Use of multi-sensor data to identify and map tropical coastal wetlands in the amazon of Northern Brazil. Wetlands 31, 11–23. https://doi.org/10.1007/s13157-010-0135-6

Ronneberger, O., Fischer, P., Brox, T., 2015. U-Net: Convolutional Networks for Biomedical Image Segmentation. pp. 234–241. https://doi.org/10.1007/978-3-319-24574-4_28

Savitzky, A., Golay, M.J.E., 1964. Smoothing and Differentiation of Data by Simplified Least Squares Procedures. Anal. Chem. 36, 1627–1639. https://doi.org/10.1021/ac60214a047

Schaeffer-Novelli, Y., Cintrón-Molero, G., Adaime, R.R., de Camargo, T.M., 1990. Variability of mangrove ecosystems along the Brazilian coast. Estuaries 13, 204–218. https://doi.org/10.2307/1351590

Sessegolo, G.C., Lana, P.C., 1991. Decomposition of Rhizophora mangle, Avicennia schaueriana and Lagunculana racemosa Leaves in a Mangrove of Paranaguá Bay (Southeastern Brazil). Bot. Mar. 34, 285–289.

Sheriza, M.R., Radzi, M.A., Marin, A., Samdin, Z., 2021. A bibliometric analysis of tropical mangrove forest land use change from 2010 to 2020. Environ. Dev. Sustain. https://doi.org/10.1007/s10668-021-01935-7

Sun, Y., Huang, J., Ao, Z., Lao, D., Xin, Q., 2019. Deep learning approaches for the mapping of tree species diversity in a tropical wetland using airborne LiDAR and high-spatial-resolution remote sensing images. Forests 10. https://doi.org/10.3390/F10111047

Tan, M., Le, Q. V., 2019. EfficientNet: Rethinking Model Scaling for Convolutional Neural Networks, in: Proceedings of the 36th International Conference on Machine Learning. Long Beach, California, USA, pp. 6105–6114.

Thakur, S., Mondal, I., Ghosh, P.B., Das, P., De, T.K., 2020. A review of the application of multispectral remote sensing in the study of mangrove ecosystems with special emphasis on image processing techniques. Spat. Inf. Res. 28, 39–51. https://doi.org/10.1007/s41324-019-00268-y

Thomas, N., Lucas, R., Bunting, P., Hardy, A., Rosenqvist, A., Simard, M., 2017. Distribution and drivers of global mangrove forest change, 1996-2010. PLoS One 12, 1–14. https://doi.org/10.1371/journal.pone.0179302

Torbick, N., Ledoux, L., Salas, W., Zhao, M., 2016. Regional mapping of plantation extent using

multisensor imagery. Remote Sens. 8. https://doi.org/10.3390/rs8030236

Vali, A., Comai, S., Matteucci, M., 2020. Deep Learning for Land Use and Land Cover Classification Based on Hyperspectral and Multispectral Earth Observation Data: A Review. Remote Sens. 12, 2495. https://doi.org/10.3390/rs12152495

Walfir, P., Filho, M.S., Paradella, W.R., 2005. Souza Filho and Paradela - Use of RS1 fine mode and Landsat-5 TM PCA for geomorphological mapping in a microtidal mangrove coast in the Amazon region - 2005.pdf 31, 214–224.

Walters, B.B., Rönnbäck, P., Kovacs, J.M., Crona, B., Hussain, S.A., Badola, R., Primavera, J.H., Barbier, E., Dahdouh-Guebas, F., 2008. Ethnobiology, socio-economics and management of mangrove forests: A review. Aquat. Bot. 89, 220–236. https://doi.org/10.1016/j.aquabot.2008.02.009

Wan, L., Zhang, H., Lin, G., Lin, H., 2019. A small-patched convolutional neural network for mangrove mapping at species level using high-resolution remote-sensing image. Ann. GIS 25, 45–55. https://doi.org/10.1080/19475683.2018.1564791

Wan, L., Zhang, H., Liu, M., Lin, Y., Lin, H., 2021. Early Monitoring of Exotic Mangrove Sonneratia in Hong Kong Using Deep Convolutional Network at Half-Meter Resolution. IEEE Geosci. Remote Sens. Lett. 18, 203–207. https://doi.org/10.1109/LGRS.2020.2969522

Wang, L., Jia, M., Yin, D., Tian, J., 2019. A review of remote sensing for mangrove forests: 1956–2018. Remote Sens. Environ. 231. https://doi.org/10.1016/j.rse.2019.111223

Xia, J., Yokoya, N., Pham, T.D., 2020. Probabilistic mangrove species mapping with multiple-source remote-sensing datasets using label distribution learning in Xuan Thuy National Park, Vietnam. Remote Sens. 12, 1–17. https://doi.org/10.3390/rs12223834

Xiao, H., Su, F., Fu, D., Lyne, V., Liu, G., Pan, T., Teng, J., 2021. Optimal and robust vegetation mapping in complex environments using multiple satellite imagery: Application to mangroves in Southeast Asia. Int. J. Appl. Earth Obs. Geoinf. 99, 102320. https://doi.org/10.1016/j.jag.2021.102320

Yi, Y., Zhang, Z., Zhang, W., Zhang, C., Li, W., Zhao, T., 2019. Semantic Segmentation of Urban Buildings from VHR Remote Sensing Imagery Using a Deep Convolutional Neural Network. Remote Sens. 11, 1774. https://doi.org/10.3390/rs11151774

Yu, H., Yang, Z., Tan, L., Wang, Y., Sun, W., Sun, M., Tang, Y., 2018. Methods and datasets on semantic segmentation: A review. Neurocomputing 304, 82–103. https://doi.org/10.1016/j.neucom.2018.03.037

Zhang, Y., Qiu, Z., Yao, T., Liu, D., Mei, T., 2018. Fully Convolutional Adaptation Networks for Semantic Segmentation, in: 2018 IEEE/CVF Conference on Computer Vision and Pattern Recognition. IEEE, Salt Lake City, UT, USA, pp. 6810–6818. https://doi.org/10.1109/CVPR.2018.00712

Zhao, C., Qin, C., 2021. A detailed mangrove map of China for 2019 derived from Sentinel-1 and -2 images and Google Earth images. Geosci. Data J. gdj3.119. https://doi.org/10.1002/gdj3.119

Zhao, C., Qin, C.Z., 2020. 10-m-resolution mangrove maps of China derived from multi-source and multi-temporal satellite observations. ISPRS J. Photogramm. Remote Sens. 169, 389–405. https://doi.org/10.1016/j.isprsjprs.2020.10.001

Zimudzi, E., Sanders, I., Rollings, N., Omlin, C.W., 2021. Remote sensing of mangroves using unmanned aerial vehicles: current state and future directions. J. Spat. Sci. 66, 195–212. https://doi.org/10.1080/14498596.2019.1627252